Hindawi Publishing Corporation
International Journal of Aerospace Engineering
Volume 2014, Article ID 432970, 12 pages
http://dx.doi.org/10.1155/2014/432970

Research Article

Active Vibration Control of Plate Partly Treated with ACLD Using Hybrid Control

Dongdong Zhang and Ling Zheng

State Key Laboratory of Mechanical Transmission, Chongqing University, Chongqing 400030, China

Correspondence should be addressed to Ling Zheng; zling@cqu.edu.cn

Received 26 December 2013; Accepted 23 June 2014; Published 14 July 2014

Academic Editor: N. Ananthkrishnan

A finite element model of plate partly treated with ACLD treatments is developed based on the constitutive equations of elastic, piezoelectric, viscoelastic materials and Hamilton's principle. The Golla-Hughes-Mctavish (GHM) method is employed to describe the frequency-dependent characteristics of viscoelastic material (VEM). A model reduction is completed by using iterative dynamic condensation and balance model reduction method to design an effective control system. The emphasis is concerned on hybrid (combined feedback/feedforward) control system to attenuate the vibration of plates with ACLD treatments. The optimal linear quadratic Gaussian (LQG) controller is considered as a feedback channel and the adaptive filtered-reference LMS (FxLMS) controller is used as a feedforward channel. They can be utilized individually or in a hybrid way to suppress the vibration of plate/ACLD system. The results show that the hybrid controller which combines feedback/feedforward together can reduce the displacement amplitude of plate/ACLD system subjected to a complicated disturbance substantially without requiring more control effort. Furthermore, the hybrid controller has more rapid and stable convergence rate than the adaptive feedforward FxLMS controller. Meanwhile, perfect robustness to phase error of the cancellation path in feedforward controller and the weight matrices in feedback LQG controller is demonstrated in proposed hybrid controller. Therefore, its application in structural engineering can be highly appreciated.

1. Introduction

Vibration and noise control is of great interest in many industrial structures, like airplane passenger cabin, vehicle body structure, and submarine hull. The thin-wall structure is a key part in the body/cabin/hull structure. The vibrating thin-wall structures, like plates and shells, which are mainly disturbed by the harmonic disturbance induced from the engine and other rotating machines, as well as stochastic disturbance, make radiation noise into the passenger cabin, influencing the performance of the structure.

Active vibration control (AVC) [1], which is well-known for its efficiency in low frequency band where traditional passive strategies cannot work well, has been applied to various structures over the past two decades. Active vibration control of simple structure, such as beams [2] and plates [3], was researched broadly in the open literatures. Thakkar and Ganguli [4] investigated the twist vibration control of helicopter rotor blade by using the piezoelectric actuators. Rao et al. [5] designed a H_∞ controller and demonstrated experimentally the effectiveness of multimode vibration control in the composite fin-tip of aircraft. Kwak and Yang [6] studied the suppression of vibration of ring-stiffened cylindrical shell in contact with external fluid using piezoelectric sensor and actuator.

Active constrained layer damping (ACLD) is a hybrid active-passive vibration control technique [7] which combines the advantages of conventional passive constrained layer damping (PCLD) and active vibration control (AVC). Therefore, in the same damping treatment, the broader band vibration suppression can be achieved through ACLD treatments. In recent decades, extensive efforts had been made to reduce the vibration of the thin-wall structure using ACLD treatments. Baz and Ro, as the pioneering researchers, demonstrated the feasibility of using the ACLD in controlling the vibration of rotating beams with

the ultimate goal of extending its application of attenuating the structural vibration of rotor blades [8]. The vibration control of shells [9, 10] was also investigated to extend the application of ACLD in the cabin of aircraft and submarine. In these studies, the PVDF (polyvinylidene fluoride) was served as the sensors and actuators. They use the simple proportional and derivative feedback of the transverse deflection to suppress the vibration of the base structure theoretically and experimentally. To improve the force transmissibility between piezoelectric actuator and the base structure, Liao and Wang [11] proposed an enhanced active constraining layer (EACL), and Gao and Liao [12] extended this configuration. Kumar et al. [13] added the stand-off layer (SOL) between the viscoelastic layer and the base structure to increase the viscoelastic strain and enhance the effect of the active force. In recent years, piezoelectric fiber-reinforced composite (PFRC) materials [14] and piezoelectric composites (PZC) [15, 16], which have a wide range of effective materials properties, were introduced in the ACLD treatments to serve as active constrained layer. Shah and Ray [17] focused on investigating the effect of the piezoelectric fiber orientation angle in the constrained layer on the performance of ACLD patches. In these studies, the emphasis was placed on the vibration characteristics analysis/enhancement of the performance of the ACLD treatments.

In the open literatures, much attention was paid on active control methods in the structural active/active-passive vibration control. The optimal feedback control [18], velocity feedback control [19], fuzzy logic control [3], and the H_∞ control [5] were usually employed in active vibration control (AVC). Viswamurthy and Ganguli [20] compared the global harmonic control with local blade optimal control applied to vibration control of helicopter. For active-passive ACLD/structure, Baz [21] presented a variational mathematical model for beams and a globally stable boundary controller was investigated to get the high damping characteristics over broad frequency range. Meanwhile, Baz [22] developed a H_2 robust controller based on the transfer function model of the ACLD beam. The control strategy was stable in the presence of parameter uncertainty, as well as ensured optimal disturbance rejection capabilities. Furthermore, the H infinity robust control strategy was utilized by Crassidis et al. [23] to maximize disturbance rejection capabilities over a desired frequency band. Liu et al. [24] developed a H infinity controller based on the reduced finite element model. Rodriguez [25] made a comparison of sliding mode control (SMC) with state-feedback control (LQR) applied to a partially treated ACLD beam. In these studies, the control strategies can be classified into feedback control theories. These control strategies have been shown to be more suitable in applications where the structure is disturbed by the stochastic or impulsive disturbances.

Feedforward control, which is more effective in the case where the deterministic or correlated information about the disturbance is known, is another popular control strategy. It was widely used in active vibration and noise control field [26, 27]. However, only a few feedforward theories were utilized in structural vibration control with ACLD treatments. Cao [28] employed the feedforward LMS algorithm to control the vibration of a plate treated with ACLD treatments. The finite element model was developed and ADF method was used to identify the performance of VEM. Furthermore, hybrid control of feedback and feedforward control theories were also successfully used to noise and vibration suppression [29, 30]. However, it was rarely investigated for structural vibration control with ACLD treatments. Vasques validated the effectiveness of the hybrid control strategies for ACLD beam [31].

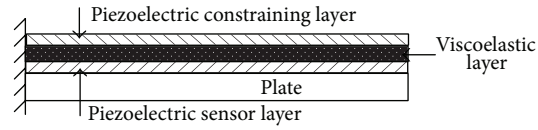

Figure 1: Schematic drawing of the ACLD/plate structure.

In this paper, the focus is placed on combining individual feedback control based on linear quadratic Gaussian (LQG) and feedforward control based on adaptive filtered-reference LMS (FxLMS), to develop a hybrid controller for the vibration control of plates treated with ACLD treatments. The performance of vibration suppression subjected to different control strategies is compared and the effect of parameters on vibration suppression of the plate with ACLD treatment is further investigated.

This paper is organized in the following five sections. A brief background is introduced in Section 1. The dynamic models including the finite element model of the plate treated with ACLD patches and GHM model of VEM are developed in Section 2. In Section 3, the feedback controller, the feedforward controller and the hybrid controller are designed. A numerical example is discussed in Section 4. Finally, the main results and future work are summarized in Section 5.

2. The ACLD/Plate System Model Construction

2.1. Finite Element Model. The ACLD/plate system is illustrated in Figure 1. The viscoelastic damping layer is sandwiched between two piezoelectric layers which serve as piezosensor and piezoactuator, respectively. The three layers are bonded to the base plate acting as a smart constraining layer damping. It is assumed that the piezosensor and the base plate are perfectly bonded together such that they can be reduced to a single equivalent layer. Some other assumptions are made in [32].

The ACLD/plate elements considered are four-node two-dimensional elements. Each node has seven degrees of freedom to describe the longitudinal displacements u_c and v_c of the constrained layer, the longitudinal displacements u_p and v_p of the base plate, the transverse deflection w, and the slopes x and y of the deflection line. The longitudinal displacement functions are expressed as 4-term polynomials, and transverse deflection w is expressed as a 12-term polynomial. Therefore, the element deflection vector is given by

$$\Delta^{(e)} = \{\Delta_1 \;\; \Delta_2 \;\; \Delta_3 \;\; \Delta_4\}^T, \tag{1}$$

where $\Delta_i = \{u_{ci} \;\; v_{ci} \;\; u_{pi} \;\; v_{pi} \;\; w_i \;\; \theta_{xi} \;\; \theta_{yi}\}^T$ for $i = 1, 2, 3, 4$.

Applying Hamilton's principle, the equations of motion for an ACLD element can be written as

$$\mathbf{M}^{(e)}\ddot{\boldsymbol{\Delta}}^{(e)} + \mathbf{K}^{(e)}\boldsymbol{\Delta}^{(e)} = \mathbf{F}_d^{(e)} + \mathbf{F}_c^{(e)}, \tag{2}$$

where $\mathbf{M}^{(e)} = \mathbf{M}_p^{(e)} + \mathbf{M}_c^{(e)} + \mathbf{M}_v^{(e)}$, $\mathbf{K}^{(e)} = \mathbf{K}_p^{(e)} + \mathbf{K}_c^{(e)} + \mathbf{K}_v^{(e)} + G_v\mathbf{K}_{v\beta}^{(e)}$, $\mathbf{M}_p^{(e)}$, $\mathbf{M}_c^{(e)}$, and $\mathbf{M}_v^{(e)}$ stand for the element mass matrices for base plate, the constrained layer, and the viscoelastic layer, $\mathbf{K}_p^{(e)}, \mathbf{K}_c^{(e)}$, and $\mathbf{K}_v^{(e)}$ stand for the element stiffness matrices for base plate, the constrained layer, and the viscoelastic layer, $\mathbf{K}_{v\beta}^{(e)}$ is the shear stiffness matrix for viscoelastic layer, G_v is the shear modulus of the viscoelastic materials, $\mathbf{F}_d^{(e)}$ is the external force vector, and $\mathbf{F}_c^{(e)}$ is the control force produced by the piezoelectric actuators.

Assembling the condensed system for all elements yields the dynamic equation of the plate with ACLD treatments:

$$\mathbf{M}\ddot{\boldsymbol{\Delta}} + \left\{\mathbf{K} + G_v\mathbf{K}_{v\beta}\right\}\boldsymbol{\Delta} = \mathbf{F}_d + \mathbf{F}_c, \tag{3}$$

where $\mathbf{K}$ is the global stiffness matrix without considering the shear stiffness of the VEM.

2.2. Viscoelastic Damping Model. The frequency- or time-dependent behavior of the viscoelastic material is characterized by using Golla-Hughes-Mctavish (GHM) method [24]. In this approach, the shear modulus of VEM is expressed as a series of "minioscillator" terms in the Laplace domain

$$sG(s) = G^{\infty}\left[1 + \sum_k \alpha_k \frac{s^2 + 2\varsigma_k\omega_k s}{s^2 + 2\varsigma_k\omega_k s + \omega^2}\right], \tag{4}$$

where G^{∞} corresponds to the equilibrium value of the modulus, constants α_k, ς_k, and ω_k govern the shape of the modulus function over the complex s-domain. A column matrix of dissipation coordinates is introduced:

$$Z'(s) = \frac{\omega^2}{s^2 + 2\varsigma\omega s + \omega^2}\Delta(s). \tag{5}$$

Considering a three-term GHM expression, (3) can be rewritten as follows:

$$\mathbf{M}'\ddot{\mathbf{X}} + \mathbf{C}'\dot{\mathbf{X}} + \mathbf{K}'\mathbf{X} = \mathbf{F}_{\mathbf{d}}' + \mathbf{F}_{\mathbf{c}}', \tag{6}$$

where each vector and matrix can be expressed as

$$\mathbf{M}' = \begin{bmatrix} \mathbf{M} & 0 & 0 & 0 \\ 0 & \frac{\alpha_1}{\omega_1^2}\boldsymbol{\Lambda} & 0 & 0 \\ 0 & 0 & \frac{\alpha_2}{\omega_2^2}\boldsymbol{\Lambda} & 0 \\ 0 & 0 & 0 & \frac{\alpha_3}{\omega_3^2}\boldsymbol{\Lambda} \end{bmatrix},$$

$$\mathbf{C}' = \begin{bmatrix} 0 & 0 & 0 & 0 \\ 0 & \frac{2\alpha_1\zeta_1}{\omega_1^2}\boldsymbol{\Lambda} & 0 & 0 \\ 0 & 0 & \frac{2\alpha_2\zeta_2}{\omega_2^2}\boldsymbol{\Lambda} & 0 \\ 0 & 0 & 0 & \frac{2\alpha_3\zeta_3}{\omega_3^2}\boldsymbol{\Lambda} \end{bmatrix},$$

$$\mathbf{K}' = \begin{bmatrix} G^{\infty}\mathbf{K}_{v\beta}\left(1 + \sum_{k=1}^{3}\alpha_k\right) + \mathbf{K}_{\mathbf{v}} & -\alpha_1\mathbf{R} & -\alpha_2\mathbf{R} & -\alpha_3\mathbf{R} \\ -\alpha_1\mathbf{R}^T & \alpha_1\boldsymbol{\Lambda} & 0 & 0 \\ -\alpha_2\mathbf{R}^T & 0 & \alpha_2\boldsymbol{\Lambda} & 0 \\ -\alpha_3\mathbf{R}^T & 0 & 0 & \alpha_3\boldsymbol{\Lambda} \end{bmatrix},$$

$$\mathbf{X} = \begin{Bmatrix} \boldsymbol{\Delta} \\ \mathbf{Z} \end{Bmatrix}, \qquad \mathbf{F}_{\mathbf{d}}' = \begin{Bmatrix} \mathbf{F}_{\mathbf{d}} \\ \mathbf{0} \end{Bmatrix}, \qquad \mathbf{F}_{\mathbf{c}}' = \begin{Bmatrix} \mathbf{F}_{\mathbf{c}} \\ \mathbf{0} \end{Bmatrix}, \tag{7}$$

where $\mathbf{K}_{v\beta} = \mathbf{R}_v\boldsymbol{\Lambda}_v\mathbf{R}_v^T$, $\boldsymbol{\Lambda} = G^{\infty}\boldsymbol{\Lambda}_v$, $\mathbf{R} = \mathbf{R}_v\boldsymbol{\Lambda}$, $\mathbf{Z} = \mathbf{R}_v^T\mathbf{Z}'$, $\boldsymbol{\Lambda}_v$ is a diagonal matrix of the positive eigenvalues of matrix $\mathbf{K}_{v\beta}$, and $\mathbf{R}_v$ is the eigenvectors matrix corresponding to the eigenvalues. For simplicity the global equation of motion can be rewritten as

$$\mathbf{M}\ddot{\mathbf{X}} + \mathbf{C}\dot{\mathbf{X}} + \mathbf{K}\mathbf{X} = \mathbf{F}_{\mathbf{d}} + \mathbf{F}_{\mathbf{c}}. \tag{8}$$

2.3. Model Reduction and State Space Design. As well known, the scale of the finite element model is increased largely due to the introduction of the dissipation coordinates from GHM model. This requires much computational effort to calculate the dynamic response of the plates with ACLD treatments. Otherwise, not all the state variables in the model are controllable and observable. Therefore, model reduction is necessary to design an effective controller. Here, an iterative dynamic condensation [33] is used to reduce the scale of the finite element model.

Equation (8) can be rewritten as

$$\begin{bmatrix} \mathbf{M}_{mm} & \mathbf{M}_{ms} \\ \mathbf{M}_{sm} & \mathbf{M}_{ss} \end{bmatrix}\begin{Bmatrix} \ddot{\mathbf{X}}_m \\ \ddot{\mathbf{X}}_s \end{Bmatrix} + \begin{bmatrix} \mathbf{C}_{mm} & \mathbf{C}_{ms} \\ \mathbf{C}_{sm} & \mathbf{C}_{ss} \end{bmatrix}\begin{Bmatrix} \dot{\mathbf{X}}_m \\ \dot{\mathbf{X}}_s \end{Bmatrix} + \begin{bmatrix} \mathbf{K}_{mm} & \mathbf{K}_{ms} \\ \mathbf{K}_{sm} & \mathbf{K}_{ss} \end{bmatrix}\begin{Bmatrix} \mathbf{X}_m \\ \mathbf{X}_s \end{Bmatrix} = \begin{Bmatrix} \mathbf{F}_m \\ \mathbf{F}_s \end{Bmatrix}. \tag{9}$$

Here, a matrix $\widehat{\mathbf{R}}$ is defined to relate the master d.o.f.s with the slave d.o.f.s and, after i iterations, the reduced dynamic equation is

$$\mathbf{M}_R^{(i)}\ddot{\mathbf{X}} + \mathbf{C}_R^{(i)}\dot{\mathbf{X}} + \mathbf{K}_R^{(i)}\mathbf{X} = \mathbf{F}_R^{(i)}, \tag{10}$$

where

$$\begin{aligned}
\mathbf{M}_R^{(i)} &= \mathbf{M}_{mm} + \mathbf{R}'^{(i)^T}\mathbf{M}_{sm} \\
&\quad + \mathbf{M}_{ms}\mathbf{R}'^{(i)} + \mathbf{R}'^{(i)^T}\mathbf{M}_{ss}\mathbf{R}'^{(i)}\mathbf{C}_R^{(i)} \\
&= \mathbf{C}_{mm} + \mathbf{R}'^{(i)^T}\mathbf{C}_{sm} + \mathbf{C}_{ms}\mathbf{R}'^{(i)} \\
&\quad + \mathbf{R}'^{(i)^T}\mathbf{C}_{ss}\mathbf{R}'^{(i)}, \\
\mathbf{K}_R^{(i)} &= \mathbf{K}_{mm} + \mathbf{R}'^{(i)^T}\mathbf{K}_{sm} \\
&\quad + \mathbf{K}_{ms}\mathbf{R}'^{(i)} + \mathbf{R}'^{(i)^T}\mathbf{K}_{ss}\mathbf{R}'^{(i)}\mathbf{F}_R^{(i)} \\
&= \mathbf{F}_m + \mathbf{R}'^{(i)^T}\mathbf{F}_s, \\
\mathbf{R}'^{(i+1)} &= -\mathbf{K}_{ss}{}^{-1}\left(\mathbf{M}_{ss}\mathbf{R}'^{(i)}\mathbf{M}_R^{(i)^{-1}}\mathbf{K}_R^{(i)} - \mathbf{K}_{sm}\right), \\
\mathbf{R}'^{(0)} &= -\mathbf{K}_{ss}^{-1}\mathbf{K}_{sm}.
\end{aligned} \tag{11}$$

Based on above reduced model, the state space form of the ACLD/plate is derived as follows:

$$\begin{aligned}
\dot{\mathbf{x}}(t) &= \mathbf{A}\mathbf{x}(t) + \mathbf{B}_d\mathbf{f}_d + \mathbf{B}_c\mathbf{f}_c, \\
\mathbf{y}(t) &= \mathbf{C}\mathbf{x}(t) + \mathbf{v},
\end{aligned} \tag{12}$$

where the state space vector $\mathbf{x}(\mathbf{t})$ is chosen as $\{\mathbf{X}_m \ \ \dot{\mathbf{X}}_m\}^T$, $\mathbf{A}$ is system matrix, and $\mathbf{B}_d$ and $\mathbf{B}_c$ are disturbance input matrices and the control force distribution matrices. $\mathbf{C}$ is the output matrix and $\mathbf{y}(\mathbf{t})$ is the output vector. $\mathbf{v}$ represents the measurement noise.

A further model reduction is performed with the balance method in the state space to guarantee the control system controllable and observable. The details are shown in [34].

3. Control System Architecture Design

3.1. Feedback Control. The ultimate aim of the feedback control is to reduce the motion of the system to the greatest possible extent; in that case, the control system is said to act as a regulator. Here, the linear quadratic regulator (LQR) is designed to control the vibration of plates with ACLD treatments. Cost function or performance index is given by

$$J = \int_0^\infty \left(\mathbf{x}(t)^T\mathbf{Q}_x\mathbf{x}(t) + \mathbf{f}_c{}^T(t)\,\mathbf{R}\mathbf{f}_c(t)\right)dt \tag{13}$$

or

$$J = \int_0^\infty \left(\mathbf{y}(t)^T\mathbf{Q}_y\mathbf{y}(t) + \mathbf{f}_c{}^T(t)\,\mathbf{R}\mathbf{f}_c(t)\right)dt, \tag{14}$$

where $\mathbf{Q}_x$, $\mathbf{Q}_y$, and $\mathbf{R}$ are the state variable, the output, and the control input weighting matrices, respectively.

The control input can be calculated using the state feedback so that

$$\mathbf{f}_c = -\mathbf{K}_c\mathbf{x}(t). \tag{15}$$

The optimal feedback gain matrix $\mathbf{K}_c$ is given by

$$\mathbf{K}_c = \mathbf{R}^{-1}\mathbf{B}_c^T\mathbf{P}, \tag{16}$$

where $\mathbf{P}$ is the solution of the famous Riccati equation.

Therefore, considering the control law in (15) and substituting it into the state space equation of the reduced model, the closed-loop state equation is given by

$$\mathbf{x}(t) = \left(\mathrm{A} - \mathbf{B}_c\mathbf{K}_c\right)\mathbf{x}(t) + \mathbf{B}_d\mathbf{f}_d. \tag{17}$$

In above equation, it is assumed that all the state variables can be measured. However that is not always available in a real system; an optimal design methodology that only utilizes noise, partial state information is required. The linear quadratic Gaussian (LQG) methodology provides a means of designing such controllers. The LQG controller is a combination of a LQR and a Kalman filter, a fact known as the separation principle.

The Kalman filter is an optimal state estimator which can minimize the effects of process and measurement noise. In (18), the process noise $\mathbf{f}_d$ and measurement noise $\mathbf{v}_d$ are both assumed to be white and have a Gaussian probability density function. Meanwhile, they are assumed to be uncorrelated with the inputs. The correlation properties of the plant and measurement noise vectors are given by the correlation matrices

$$E\left(\mathbf{f}_d\mathbf{f}_d^T\right) = Q_d, \qquad E\left(\mathbf{v}_d\mathbf{v}_d^T\right) = R_d, \tag{18}$$

where E denotes the expectation operator. These matrices are used as weighting matrices of the steady-state Kalman filter problem [20].

A state estimate $\mathbf{x}'(t)$ that minimizes the steady-state error covariance is constructed by the Kalman filter

$$P = \lim_{t\to\infty} E\left(\left[\mathbf{x}(t) - \mathbf{x}'(t)\right]\left[\mathbf{x}(t) - \mathbf{x}'(t)\right]^T\right). \tag{19}$$

In this way, a new state space model is generated

$$\begin{aligned}
\dot{\mathbf{x}}' &= \mathbf{A}\mathbf{x}' + \mathbf{B}_c\mathbf{f}_c^{fd} + \mathbf{L}\left(\mathbf{y}_v - \mathbf{C}\mathbf{x}'\right) \\
\begin{bmatrix}\mathbf{y}' \\ \mathbf{x}'\end{bmatrix} &= \begin{bmatrix}\mathbf{C} \\ \mathbf{I}\end{bmatrix}\mathbf{x}',
\end{aligned} \tag{20}$$

where $\mathbf{L}$ is the filter gain; it is determined by solving an algebraic Riccati equation; $\mathbf{y}_v$ is the sum of the output and the measurement noise.

3.2. Feedforward Control. The filtered-reference LMS (FxLMS) algorithm is widely studied and has been used in many active vibration control areas due to its easy implementation and remarkable performance. In a practical

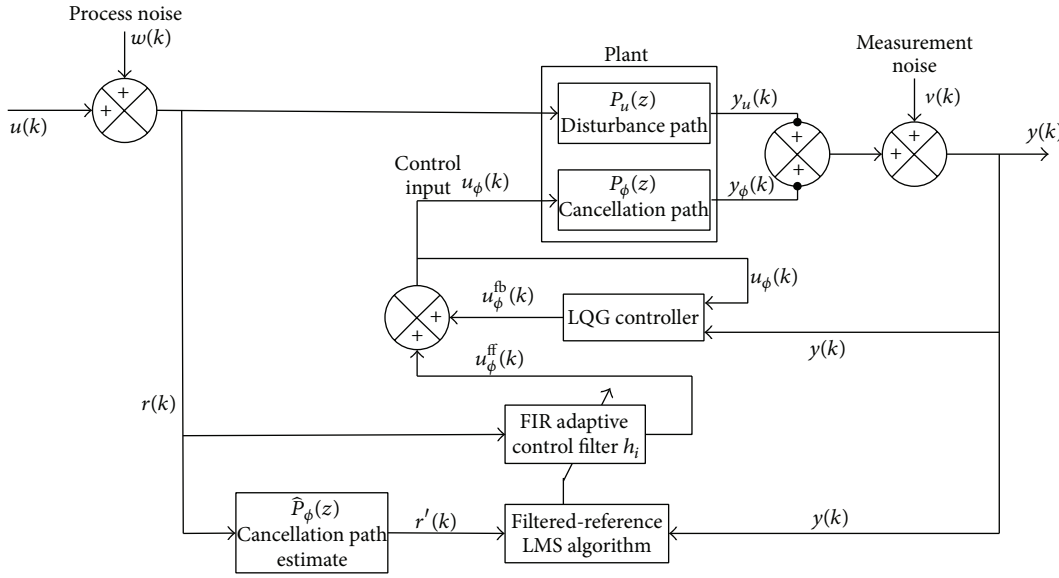

Figure 2: Schematic diagram of the generalized plant for hybrid (combined feedback/feedforward) controller.

vibration control system, a cancellation path exists, which has an important effect on the control results. In FxLMS algorithm, the model of the cancellation path is established. The primary disturbance $r(k)$ passes through the estimated model of the cancellation path, and a filtered-reference signal $r'(k)$, which is correlated with the disturbance, is produced. This signal is then adaptively filtered to generate the necessary control action f_c^{ff} to cancel the effect of the primary disturbance.

An adaptive finite impulse response (FIR) filter, whose ith coefficient at the kth sample time $h_i(k)$ is updated using the LMS algorithm, is used in filtering process. The coefficients vector $h_i(k)$ and the filter output $f_c^{ff}(k)$ are obtained from

$$\begin{aligned} h_i(k) &= h_i(k-1) + 2\mu e(k-1) r'(k-1), \\ f_c^{ff}(k) &= \sum_{i=0}^{N-1} h_i(k) r'(k-i), \end{aligned} \tag{21}$$

where μ is the step size, which has a significant influence on the convergence rate of the LMS algorithm, and N is the number of filter coefficients (or the filter length).

The control signal has to pass through a part of the physical system before the error sensor measures the output. This physical path, $P_\phi(z)$, is called the cancelation path; this transfer characteristics also affect the performance of the FxLMS algorithm. Therefore, the output of the plant due to the feedforward control input only, $y_\phi(k)$, is given by

$$y_\phi(k) = \sum_{j=0}^{M-1} g_j \sum_{i=0}^{N-1} h_i(k) r'(k-i-j), \tag{22}$$

where g_i is the discrete impulse response of the cancelation path $P_\phi(z)$ which is assumed to be of order M. Considering the measurement noise $v(k)$, the output of the system, $y(k)$, can be written as

$$y(k) = y_u(k) + \sum_{j=0}^{M-1} g_j \sum_{i=0}^{N-1} h_i(k) r'(k-i-j) + v(k), \tag{23}$$

where $y_u(k)$ is the response due to the effects of the primary disturbance alone.

3.3. Hybrid Control. In general, the feedback control is more appropriate for suppression of stochastic disturbance. Meanwhile, it is susceptible to modeling errors. By contrast, the adaptive feedforward control is not susceptible to modeling errors and inherently stable, and it is more suitable to reduce the periodic or limited-band disturbance. Therefore, it is necessary to develop a hybrid (combined feedback/feedforward) control to attenuate vibration of plates with ACLD treatments against stochastic and harmonic disturbance simultaneously. The schematic diagram of the discrete-time generalized plant for a hybrid SISO control system is shown in Figure 2. It is seen that LQG control is considered as feedback channel and an adaptive filtered-reference LMS control is used as feedforward channel.

4. Numerical Simulation and Discussion

To the first bending mode of the plate, a cantilever ACLD/plate as shown in Figure 3 is used as numerical example to demonstrate the effectiveness of the above controllers. The emphasis is on the performance discussion of the controllers.

4.1. The Numerical Model of the ACLD/Plate System. The base plate, with the size of 0.2×0.1 m^2, is partly treated with ACLD treatments. The main physical parameters of the base plate

Table 1: Geometrical and physical parameters of ACLD/plate system.

Aluminum		P-5H		ZN-1			
h_p	0.0008 m	h_c	0.0005 m	h_v	0.001 m	ς_1	148.0
E_p	69 GPa	E_c	74.5 GPa	μ_v	0.3	ς_2	12.16
μ_p	0.3	μ_c	0.32	ρ_v	789.5 kg/m^3	ς_3	810.4
ρ_p	2800 kg/m^3	ρ_c	7450 kg/m^3	G^∞	554200 Pa	ω_1	896200
		d_{31}, d_{32}	186×10^{-12} C/N	α_1	3.960	ω_2	927800
				α_2	65.69	ω_3	761300
				α_3	1.447		

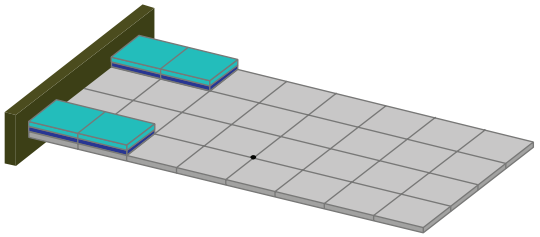

Figure 3: The schematic diagram of finite element grid for ACLD/plate.

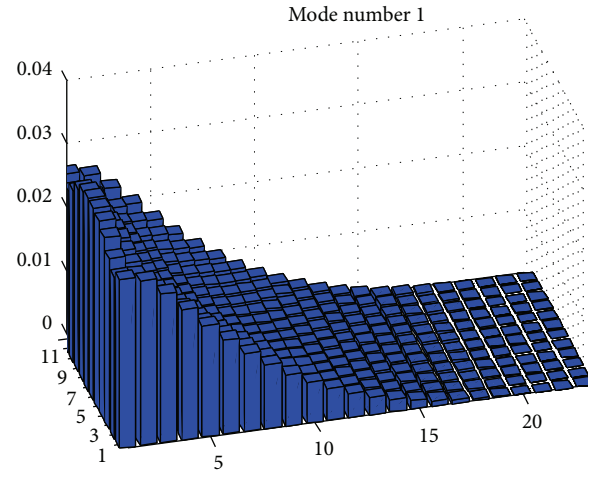

Figure 4: The modal strain energy of the first mode.

(aluminum), viscoelastic layer (ZN-1), and piezoelectric layer (P-5H) are listed in Table 1.

The cantilever plate/ACLD is divided into 8×4 elements. Four ACLD composite elements are applied in the root. The locations of the ACLD patches are decided according to the modal energy of the first mode [21], which is shown in Figure 4. A model reduction in which the deflection of the structure and displacements of the piezoelectric layer are selected to be master d.o.f.s and all others are slave d.o.f.s is performed according to the model reduction procedures in Section 3. The bold point in Figure 3 is used as the excited point and also the response point. The comparison of responses in frequency domain and time domain between the original model and the reduced model is presented in Figure 5. It is clear that the dynamic response of the reduced model is nearly coordinate with the dynamic response of the original model. A SISO control system is considered to design individual and hybrid controller. The input is the control voltage applied to the ACLD treatments, and the output is selected to be the displacement of the response point of the plate, which is assumed to be measurable.

4.2. The Control Results of the Feedback Controller. The LQG feedback controller is tested to mitigate the effects of stochastic disturbances. A white noise mechanical disturbance is modeled as process noise (input force disturbance). The process noise is such a signal with $E(ww^T) = 0.01N^2$ and the measurement noise is a signal with $E(ww^T) = 10^{-10}V^2$. The output weighting matrix is set to be $Q = 1 \times 10^6$ and the control weighting matrix $R = 1 \times 10^{-5}$. In order to avoid the depolarization, the maximum control voltage applied to piezoelectric actuators is set to be 150 V. The control results and the control voltage are presented in Figure 6.

As can be seen, when compared to the PCLD/plate system, the ACLD treatments can reduce the displacement of the response point of the plate significantly. The control voltage is limited within 30 V. This means that the proposed feedback control is effective against the stochastic disturbance.

4.3. The Control Results of the Feedforward Controller. The feedforward controller based on adaptive FxLMS algorithm is designed to attenuate the effects of the harmonic point-force disturbance on the ACLD/plate system in Figure 2. The disturbance frequency is close to the first natural frequency of the ACLD/plate system. For convenience, the estimation model of the plant cancellation path is substituted by the control path (control voltage to measured displacement) in the state space model. After that, the FxLMS algorithm is implemented. The filter length L is set to be 32 and the step size $u = 0.01$ in the FxLMS controller. The results are presented in Figure 7.

It can be seen that the displacement of the plate with ACLD treatment is attenuated from 9.4 mm to 0.08 mm at the end time of 20 s. The control voltage is close to 50 V. The vibration attenuation is improved substantially by ACLD treatments when the adaptive FxLMS algorithm is applied. It is clear that the FxLMS algorithm is very useful to attenuate the vibration of ACLD/plate system excited by harmonic disturbance.

Table 2: The convergence situation for hybrid controller and FxLMS controller under different step sizes.

	Step size μ							
	0.01	0.05	0.1	0.5	1.0	3.0	3.5	10.0
Hybrid controller	Y	Y	Y	Y	Y	Y	Y	Y
FxLMS controller	Y	Y	Y	Y	Y	Y	N	N

Y: convergence, N: no convergence.

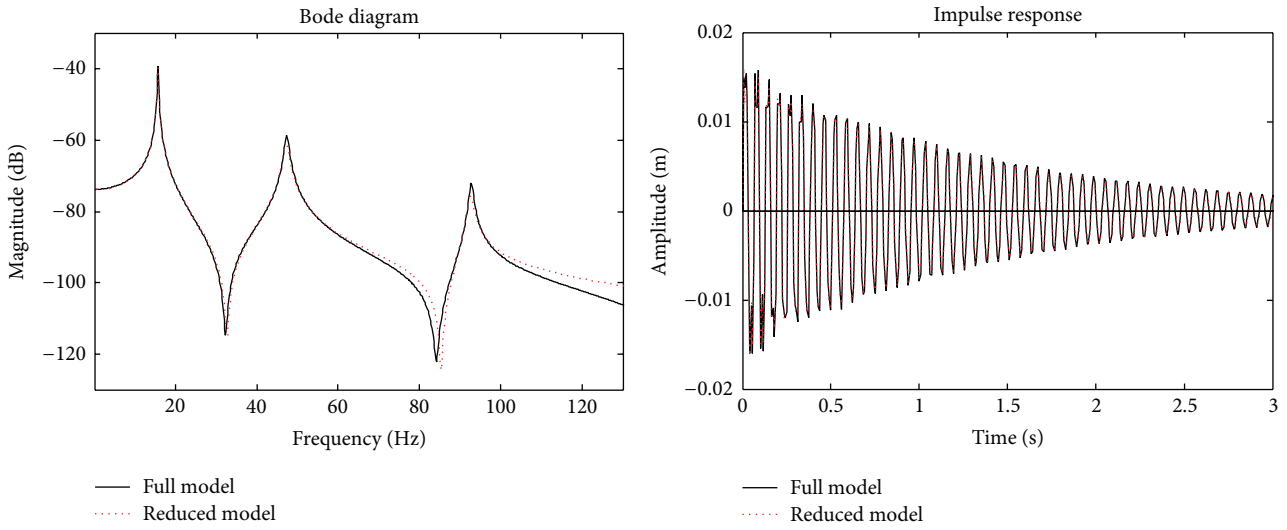

Figure 5: The frequency and time domain responses of the original and reduced model of the ACLD/plate.

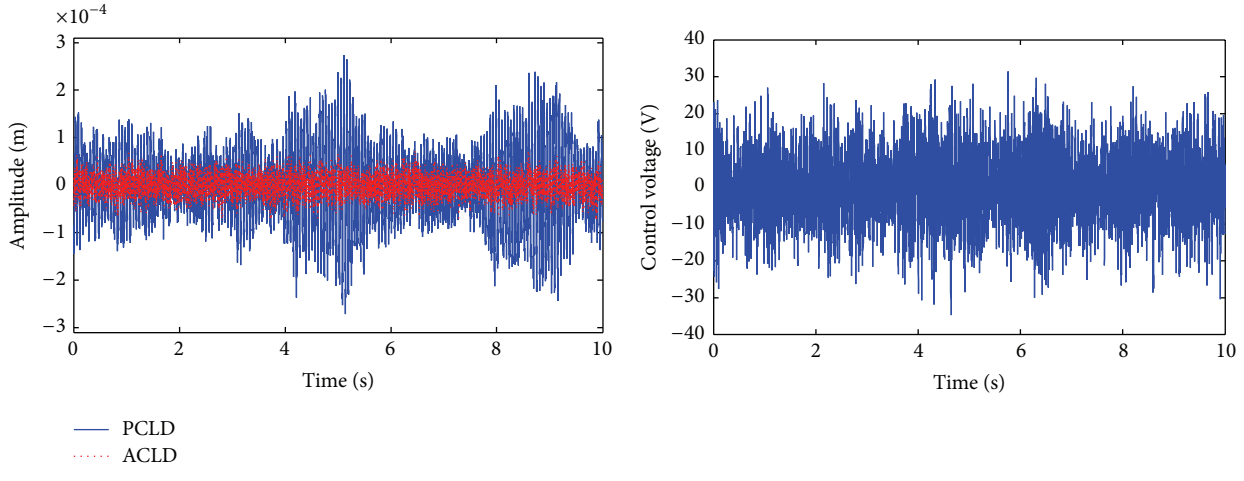

Figure 6: The displacement and control voltage for a white noise disturbance using the LQG feedback control: (a) the displacement response, (b) the control voltage.

4.4. The Control Results of the Hybrid Controller. Furthermore, it is particularly true that the system is often subject to both the harmonic and stochastic disturbances in engineering practice. Therefore, a hybrid controller, which combines the LQG feedback control and the FxLMS feedforward control together, is developed. Such a hybrid controller is further designed to attenuate the vibration of the plate/ACLD system subjected to the complicated disturbance. In the hybrid controller, the FxLMS control is employed as the feedforward channel, which aims to damp out the harmonic disturbance. Meanwhile, the LQG feedback control is used as a compensator. The mixed disturbance is the sum of

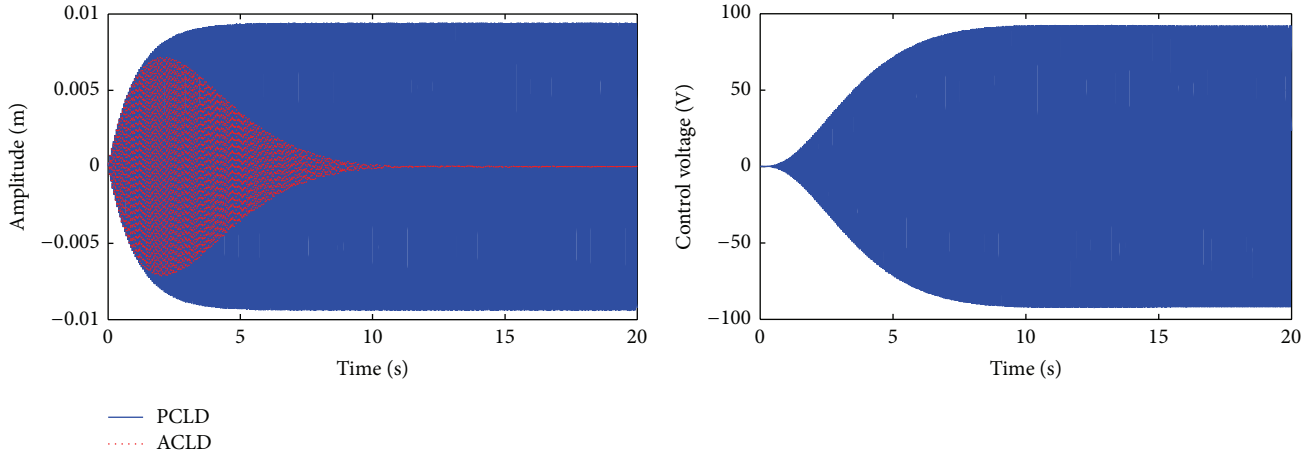

Figure 7: The displacement, control voltage for a single frequency harmonic disturbance using the adaptive filtered-reference LMS feedforward control: (a) the displacement response, (b) the control voltage.

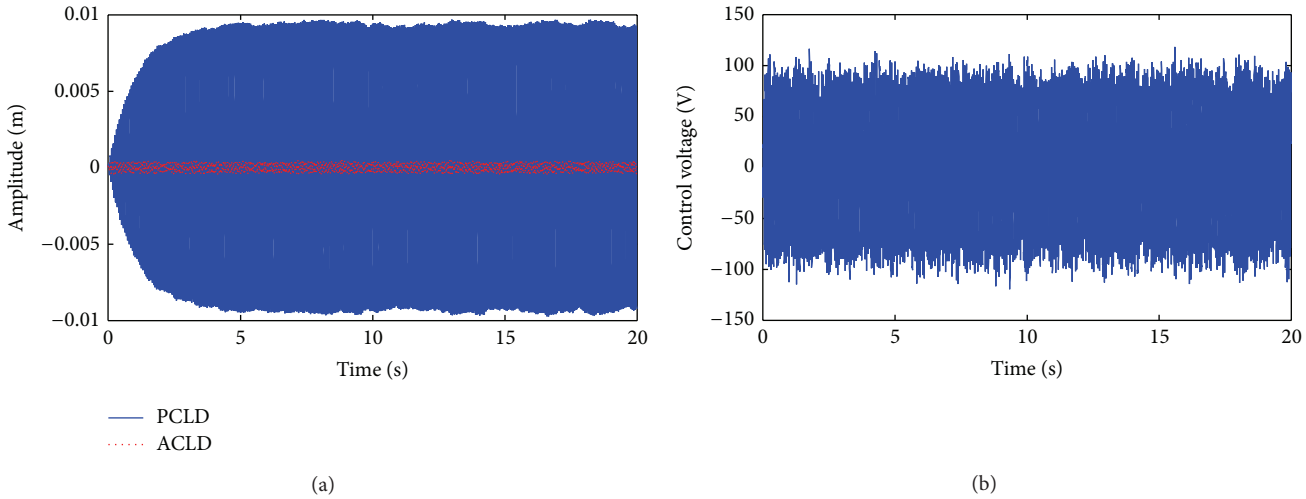

Figure 8: The displacement response for a mixed disturbance using the LQG feedback controller: (a) the displacement response, (b) the control voltage.

the two previous disturbances. The results of individual LQG feedback control, feedforward control, and their combination are presented in Figures 8, 9, and 10, respectively.

When the hybrid control system is engaged, the feedback controller with the same weights and the feedforward controller with the same filter length are used, and the step size is set to be 0.5 to accelerate the convergence rate. It can be seen from Figures 8(a) and 10(a) that at the end of 20 s, the displacement amplitude produced by the hybrid controller is much smaller than that of the LQG feedback controller. It is also apparent that the fluctuation disappears during the convergence process and the convergence rate is improved from 10 s to 5 s when the hybrid controller is applied instead of the feedforward controller. Figure 11 shows that the hybrid control produces a smaller MSE than the feedforward control. The maximum control voltage in the feedforward controller achieves 210 V. However, the control effort in the hybrid controller is only about 110 V, a little larger than the stable control voltage of the two single controller.

4.5. The Performance Discussions to the Controllers. Table 2 lists the convergence situations for hybrid controller and FxLMS controller under different step sizes. It can be seen that the hybrid controller can converge over a larger range of step size. This implies that the hybrid controller has a better robustness than the FxLMS controller.

The effect of different step sizes on the performance of ACLD/plate with the FxLMS and hybrid controller is discussed. It is seen in Figure 12 that when the step size is increased, MSE decreases rapidly; meanwhile, the fluctuation increases. This means that convergence process is not smooth anymore, which results in the fluctuation of the control voltage shown in Figure 9(b). On the other hand, at the end

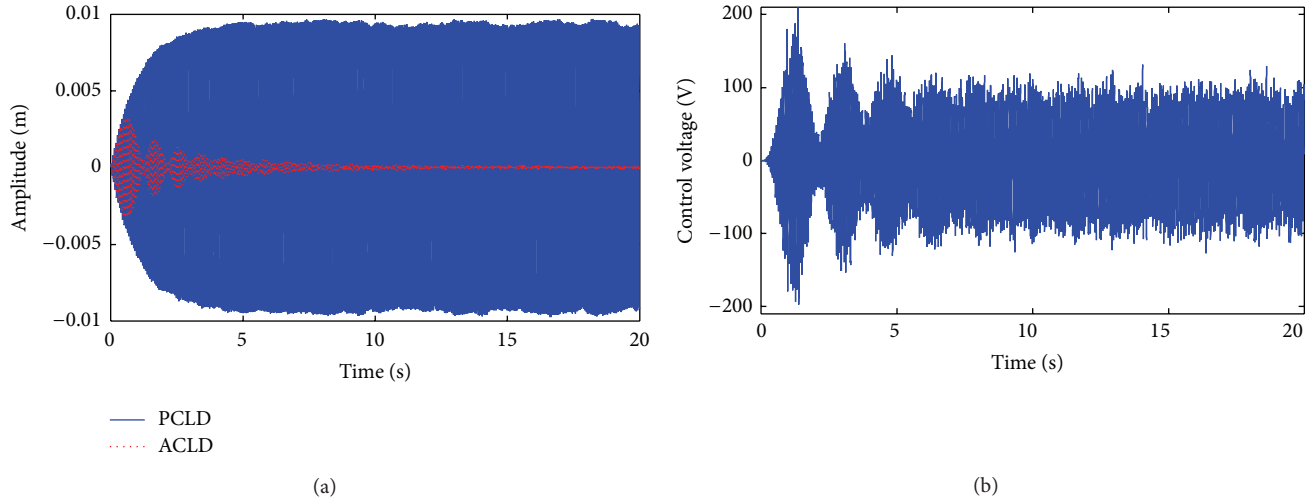

Figure 9: The displacement response for a mixed disturbance using the FxLMS feedforward controller: (a) the displacement response, (b) the control voltage.

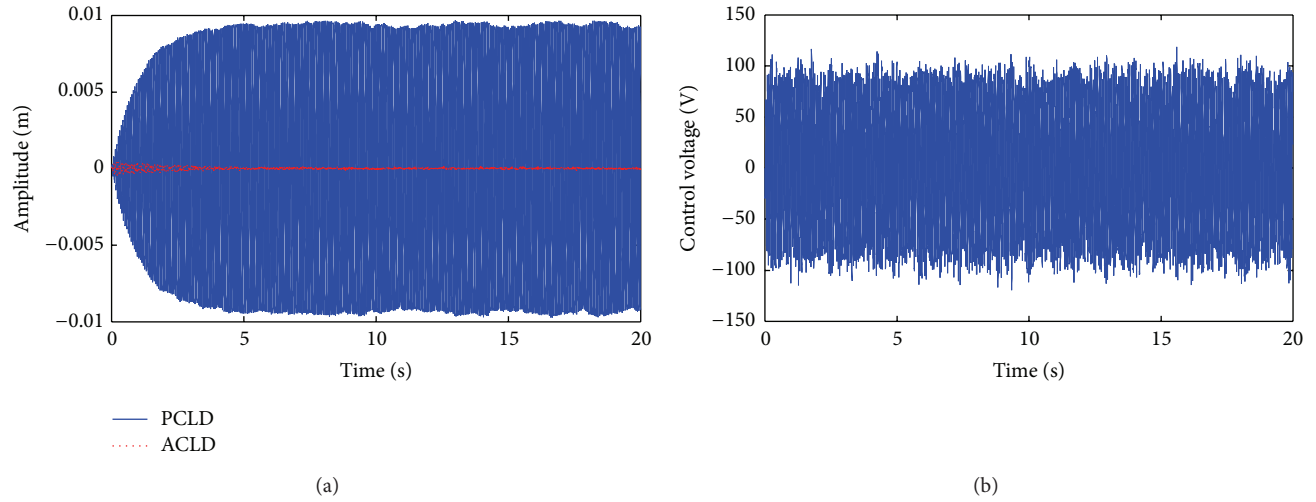

Figure 10: The displacement response for a mixed disturbance using the hybrid controller: (a) the displacement response, (b) the control voltage.

of the iteration process, the MSE approaches to the same value. Figure 13 shows that MSE varies with iteration number in hybrid control under different step sizes. It can be seen clearly that the fluctuation is reduced substantially in the convergence process and the convergence rate is improved greatly when the step size increases. This results in a stable control voltage in Figure 10(b).

In general, the cancellation path model of the feedforward controller is obtained by the system identification algorithm. Therefore, the errors including amplitude error and phase error in the cancellation path has a significant effect on the controller performance. Figures 14 and 15 show that the effect of phase errors of the cancellation path on the performance of ACLD/plate is considerable. It is seen that when the phase error achieves 30°, the control process in feedforward control will not converge anymore. However, when the phase error achieves 60°, the control process is still convergent in the hybrid control. It can be concluded that the hybrid control is not sensitive to the phase error, compared with the feedforward control.

Figure 16 shows the MSE using LQG feedback control under different Q matrix. Figure 17 demonstrates the MSE by using hybrid control under different Q matrix. It can be found that the performance of the feedback control has a distinct fluctuation when different Q matrix is applied. However, the performance of the hybrid control changes indistinctively. That implies that the hybrid control is more stable than individual LQG control.

Based on the above discussions, it can be inferred that the hybrid control will be a potential for vibration control of aerospace and other structures. The hybrid controller demonstrates a better performance than that of individual feedback/feedforward controller with different parameters. Meanwhile, even though one of individual controllers is out

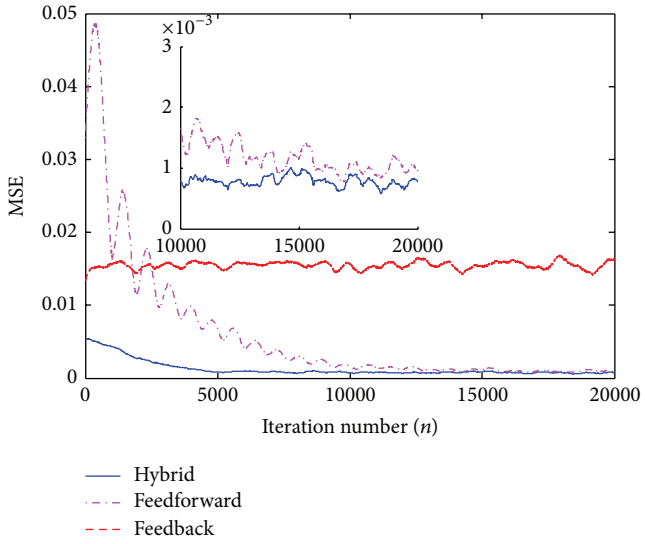

FIGURE 11: The MSE using the feedforward control, feedback control, and hybrid control.

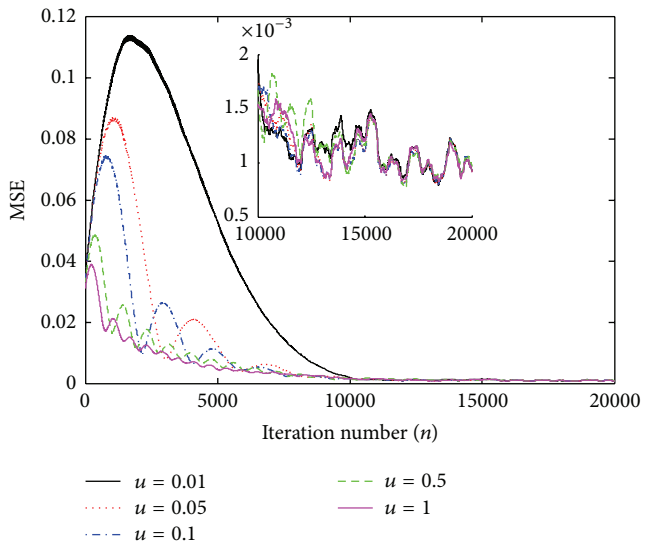

FIGURE 12: The MSE using the feedforward control under different step sizes.

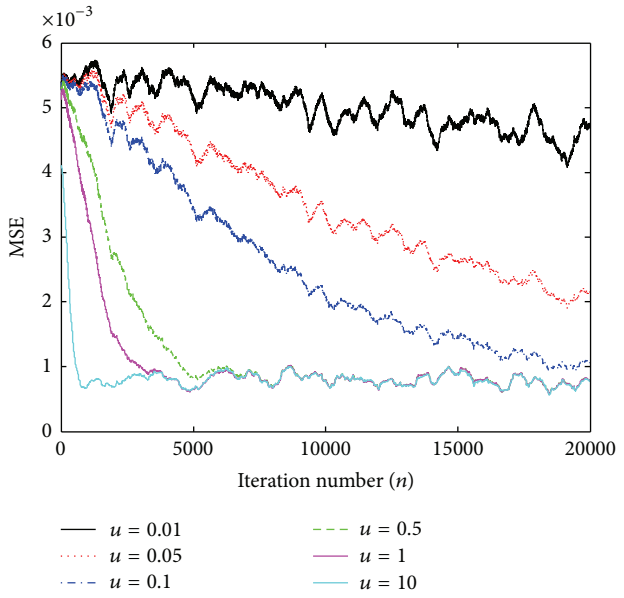

FIGURE 13: The MSE using the hybrid control under different step sizes.

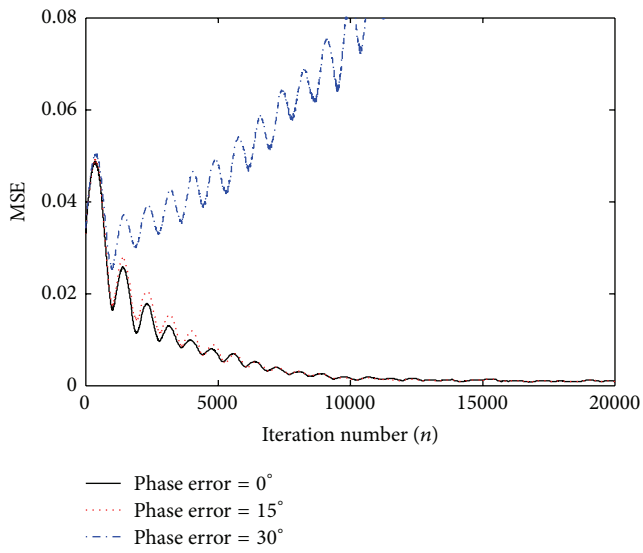

FIGURE 14: The MSE using the feedforward control under different phase errors of the cancellation path.

of work, the other will still be effective on suppressing the vibration of structure. However, it is reasonable that the modeling accuracy of the cancellation path will make an influence on performance for vibration control in practical applications.

5. Conclusions

In this paper, a finite element model of ACLD/plate system is developed. The behavior of the viscoelastic material is modeled by the Golla-Hughes-Mctavish (GHM) method. The model reduction is carried out by means of dynamic condensation and balance reduction methods, respectively, to design an effective control system. The emphasis has been placed on vibration control of ACLD/plate using the hybrid controller which is composed of the LQG feedback controller and the adaptive FxLMS feedforward controller. The performance of these controllers with different parameters is further discussed in detail.

The results show that the reduction process is effective in low frequency range. The LQG feedback controller is very useful to attenuate the vibration of the ACLD/plate system against stochastic disturbance, while the adaptive FxLMS feedforward controller is more appropriate to attenuate the vibration of the ACLD/plate system induced by harmonic disturbance. Furthermore, the LQG feedback controller and

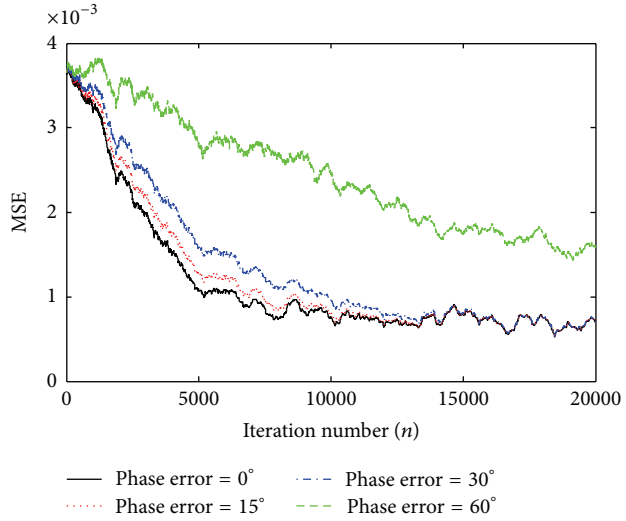

Figure 15: The MSE using the hybrid control under different phase errors of the cancellation path.

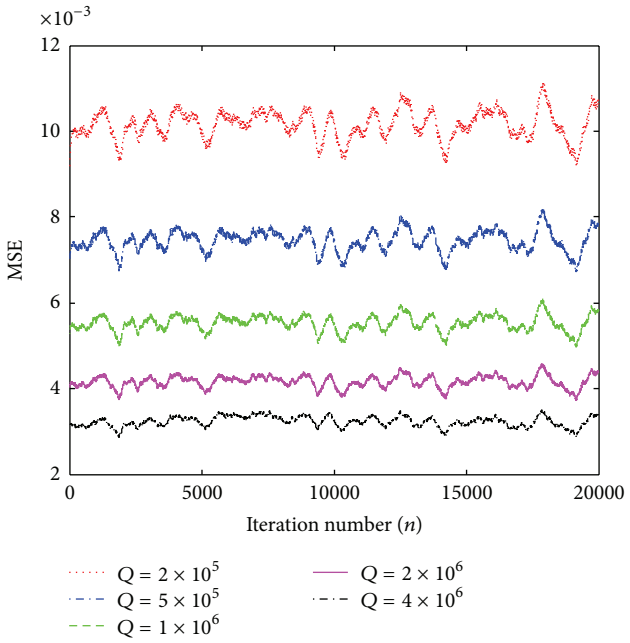

Figure 16: The MSE using the LQG feedback control under different Q matrix.

the adaptive FxLMS feedforward controller are combined as the hybrid controller, which can reduce substantially the displacement amplitude of plate/ACLD system subjected to a complicated disturbance without requiring more control effort and is more stable and smooth. On the other hand, the hybrid controller demonstrates a rapider and more stable convergence rate than the adaptive feedforward controller. Meanwhile, the hybrid controller demonstrates much better robustness than individual LQG feedback control or adaptive feedforward control.

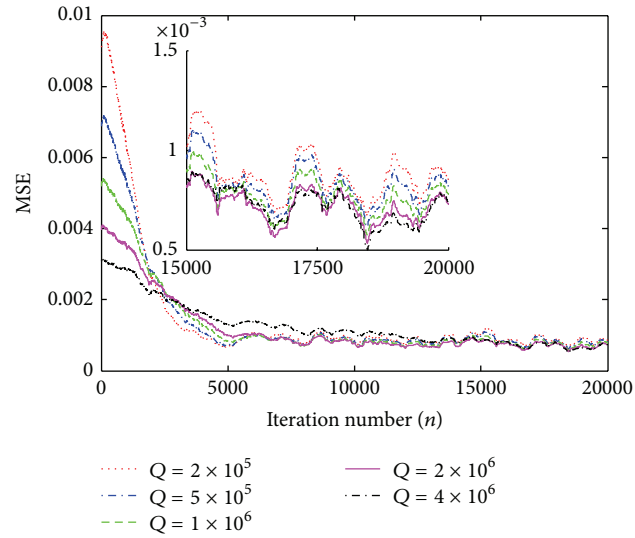

Figure 17: The MSE using the hybrid control under different Q matrix.

It is worth mentioning that although the hybrid controller presented is shown theoretically with better performance for a single mode vibration control, the research for SISO/MIMO vibration control of several modes using hybrid control strategies is more applicable in practical flexible structures of aerospace and other engineering fields. An attempt to address these issues is recommended to future studies.

Conflict of Interests

The authors declare that there is no conflict of interests regarding the publication of this paper.

Acknowledgments

This work was supported by Nature Science Foundation of China (no. 50775225), the State Key Laboratory of Mechanical Transmission, Chongqing University (no. 0301002109165). These financial supports are gratefully acknowledged.

References

[1] R. C. Fuller, J. S. Elliott, and A. P. Nelson, *Active Control of Vibration*, Academic Press, London, UK, 1997.

[2] C. M. A. Vasques and J. D. Rodrigues, "Active vibration control of smart piezoelectric beams: comparison of classical and optimal feedback control strategies," *Computers & Structures*, vol. 84, no. 22-23, pp. 1402–1414, 2006.

[3] A. H. N. Shirazi, H. R. Owji, and M. Rafeeyan, "Active vibration control of an FGM rectangular plate using fuzzy logic controllers," *Procedia Engineering*, vol. 14, pp. 3019–3026, 2011.

[4] D. Thakkar and R. Ganguli, "Induced shear actuation of helicopter rotor blade for active twist control," *Thin-Walled Structures*, vol. 45, no. 1, pp. 111–121, 2007.

[5] A. K. Rao, K. Natesan, M. S. Bhat, and R. Ganguli, "Experimental demonstration of H_∞ control based active vibration suppression in composite fin-tip of aircraft using optimally placed

piezoelectric patch actuators," *Journal of Intelligent Material Systems and Structures*, vol. 19, no. 6, pp. 651–669, 2008.

[6] M. K. Kwak and D. H. Yang, "Active vibration control of a ring-stiffened cylindrical shell in contact with unbounded external fluid and subjected to harmonic disturbance by piezoelectric sensor and actuator," *Journal of Sound and Vibration*, vol. 332, no. 20, pp. 4775–4797, 2013.

[7] A. Benjeddou, "Advances in hybrid active-passive vibration and noise control via piezoelectric and viscoelastic constrained layer treatments," *Journal of Vibration and Control*, vol. 7, no. 4, pp. 565–602, 2001.

[8] A. Baz and J. Ro, "Vibration control of rotating beams with active constrained layer damping," *Smart Materials and Structures*, vol. 10, no. 1, pp. 112–120, 2001.

[9] M. C. Ray, J. Oh, and A. Baz, "Active constrained layer damping of thin cylindrical shells," *Journal of Sound and Vibration*, vol. 240, no. 5, pp. 921–935, 2001.

[10] T. H. Chen, *Vibration control of cylindrical shells with active constrained layer damping [Ph.D. thesis]*, Catholic University, Washington, DC, USA, 1996.

[11] W. H. Liao and K. W. Wang, "On the active-passive hybrid control actions of structures with active constrained layer treatments," *Journal of Vibration and Acoustics, Transactions of the ASME*, vol. 119, no. 4, pp. 563–571, 1997.

[12] J. X. Gao and W. H. Liao, "Vibration analysis of simply supported beams with enhanced self-sensing active constrained layer damping treatments," *Journal of Sound and Vibration*, vol. 280, no. 1-2, pp. 329–357, 2005.

[13] S. Kumar, R. Kumar, and R. Sehgal, "Enhanced ACLD treatment using stand-off-layer: FEM based design and experimental vibration analysis," *Applied Acoustics*, vol. 72, no. 11, pp. 856–872, 2011.

[14] J. Shivakumar, M. H. Ashok, and M. C. Ray, "Active control of geometrically nonlinear transient vibrations of laminated composite cylindrical panels using piezoelectric fiber reinforced composite," *Acta Mechanica*, vol. 224, no. 1, pp. 1–15, 2013.

[15] P. H. Shah and M. C. Ray, "Active control of laminated composite truncated conical shells using vertically and obliquely reinforced 1-3 piezoelectric composites," *European Journal of Mechanics A/Solids*, vol. 32, pp. 1–12, 2012.

[16] M. C. Ray and J. N. Reddy, "Active damping of laminated cylindrical shells conveying fluid using 1–3 piezoelectric composites," *Composite Structures*, vol. 98, pp. 261–271, 2013.

[17] P. H. Shah and M. C. Ray, "Active structural-acoustic control of laminated composite truncated conical shells using smart damping treatment," *Journal of Vibration and Acoustics, Transactions of the ASME*, vol. 135, no. 2, Article ID 021001, 2013.

[18] M. V. Kumar, P. Sampath, S. Suresh, S. N. Omkar, and R. Ganguli, "Design of a stability augmentation system for a helicopter using LQR control and ADS-33 handling qualities specifications," *Aircraft Engineering and Aerospace Technology*, vol. 80, no. 2, pp. 111–123, 2008.

[19] J. Rohlfing, P. Gardonio, and D. J. Thompson, "Comparison of decentralized velocity feedback control for thin homogeneous and stiff sandwich panels using electrodynamic proof-mass actuators," *Journal of Sound and Vibration*, vol. 330, no. 5, pp. 843–867, 2011.

[20] S. R. Viswamurthy and R. Ganguli, "Performance sensitivity of helicopter global and local optimal harmonic vibration controller," *Computers and Mathematics with Applications*, vol. 56, no. 10, pp. 2468–2480, 2008.

[21] A. Baz, "Boundary control of beams using active constrained layer damping," *Journal of Vibration and Acoustics*, vol. 119, no. 2, pp. 166–172, 1997.

[22] A. Baz, "Robust control of active constrained layer damping," *Journal of Sound and Vibration*, vol. 211, no. 3, pp. 467–480, 1998.

[23] J. L. Crassidis, A. Baz, and N. Wereley, "H_{∞} control of active constrained layer damping," *Journal of Vibration and Control*, vol. 6, no. 1, pp. 113–136, 2000.

[24] T. Liu, H. Hua, and Z. Zhang, "Robust control of plate vibration via active constrained layer damping," *Thin-Walled Structures*, vol. 42, no. 3, pp. 427–448, 2004.

[25] J. J. Rodriguez, *Comparison of sliding mode and state feedback control applied to a partilly treated actively damped beam [M.S. thesis]*, University of Texas, Austin, Tex, USA, 2006.

[26] P. Belanger, A. Berry, Y. Pasco, O. Robin, Y. St-Amant, and S. Rajan, "Multi-harmonic active structural acoustic control of a helicopter main transmission noise using the principal component analysis," *Applied Acoustics*, vol. 70, no. 1, pp. 153–164, 2009.

[27] L. Lei, Z. Gu, and M. Lu, "MIMO hybrid control of structural responses for helicopter," *Chinese Journal of Aeronautics*, vol. 16, no. 3, pp. 151–156, 2003.

[28] Y. Q. Cao, *Study on vibration and noise control for car body structure based on smart constrained layer damping [Ph.D. thesis]*, Chongqing University, Chongqing, China, 2011.

[29] W. R. Saunders, H. H. Robertshaw, and R. A. Burdisso, "A hybrid structural control approach for narrow-band and impulsive disturbance rejection," *Noise Control Engineering Journal*, vol. 44, no. 1, pp. 11–21, 1996.

[30] D. P. Man and A. Preumont, "Hybrid feedback-feedforward control for vibration suppression," *Journal of Structure Control*, vol. 3, no. 1-2, pp. 33–44, 1996.

[31] H. Kim and H. Adeli, "Hybrid feedback-least mean square algorithm for structural control," *Journal of Structural Engineering*, vol. 130, no. 1, pp. 120–127, 2004.

[32] Z. Ling, L. Zheng, and Y. Wang, "Vibration and damping characteristics of cylindrical shells with active constrained layer damping treatments," *Smart Materials and Structures*, vol. 20, no. 2, pp. 1–9, 2011.

[33] Z. Q. Qu, "A multi-step method for matrix condensation of finite element models," *Journal of Sound and Vibration*, vol. 214, no. 5, pp. 965–971, 1998.

[34] M. J. Lam, D. J. Inman, and W. R. Saunders, "Hybrid damping models using the Golla-Hughes-McTavish method with internally balanced model reduction and output feedback," *Smart Materials and Structures*, vol. 9, no. 3, pp. 362–373, 2000.